"Healthcare Chip Checking Health Condition from Analysis of Trace Blood Collected by Painless Needle", *Jpn. Appl. Phys.*, 42, pp.3722–3727 (2003)

3）*Handbook of Optical Biomedical Diagnostics*, V.V.Tuchin ed. SPIE press p.425

4）H.Ogawa, M.Nagai, J.Kikuchi and Y.Horiike, "Blood Painless Collection System Equipping Detection functions for Search of Vein", in : M.A.Northrup, K.F.Jensen, D.J.Harrison (Eds.), Proc. μTAS2003, Squaw Valley USA, pp. 741–744 (2003)

Japanese Journal of Applied Physics
Vol. 44, No. 7A, 2005, pp. 5275–5277


**Brief Communication**

# RF Attenuation Characteristics for *In Vivo* Wireless Healthcare Chip

Tomohiro YAMADA*, Takumi UEZONO, Kenichi OKADA, Kazuya MASU, Akio OKI[1] and Yasuhiro HORIIKE[1]

*Precision and Intelligence Laboratory, Tokyo Institute of Technology, 4259-R2-17 Nagatsuta, Midori-ku, Yokohama 226-8503, Japan*
[1]*Biomaterials Center, National Institute for Materials Science, 1-1 Namiki, Tsukuba, Ibaraki 305-0044, Japan*

(Received January 6, 2005; accepted April 8, 2005; published July 8, 2005)

We investigate a wireless communication system for an *in vivo* healthcare chip. In this paper, we present measured attenuation characteristics through the human body at several frequencies. In the measurement, we use physiological saline and fresh meat instead of a real human body. From the measured results, we found that 13.56 MHz has an attenuation of 47 dB and is suitable for the proposed system. [DOI: 10.1143/JJAP.44.5275]

KEYWORDS: antenna, attenuation characteristics, wireless communication, *in vivo* chip, healthcare

Recently, several remote sensing systems for the human body have been proposed to transmit medical data and images.[1,2] We are studying a small-size healthcare system which uses wireless communication through the human body as shown in Fig. 1.[3] It consists of measuring sensors, an RF circuit, an antenna, and an energy supply. The proposed system uses a device that is battery-less and smaller than conventional devices. To use the proposed system, one must swallow the device like a tablet. The medical information is measured in the body, and the measured results are transmitted to outside of the human body. Recently, numerous bio-MEMS sensors have been proposed, which enables us to gather various medical information, such as stomach pH, and internal body temperature.[4]

The purpose of this work is to determine an appropriate frequency for *in vivo* wireless communication without a battery. Attenuation is one of the most important issues for the proposed system, because the transmitting power has to be small from the viewpoint of medical safety to the body. Several measurements of the attenuation characteristics have been reported.[5] However, the attenuation depends on the structure and spatial arrangement of antenna coils. The attenuation characteristics are very important in designing the wireless communication system. Attenuation characteristics have to be measured for each communication system.

We use physiological saline (0.9% salt solution) and fresh meat instead of the human body in the measurement. This paper reports attenuation characteristics at several frequencies: 300 kHz, 1 MHz, 3.5 MHz, 13 MHz, 35 MHz, and 2.45 GHz.

Electromagnetic radiation generates near and far fields. In the far field, the electromagnetic power is transmitted as an electromagnetic wave. In the near field, the power is transmitted by electric and magnetic coupling, *e.g.*, electromagnetic coupling transmission. The transmitting distance of the near field depends on the signal wavelength. When the transmitting distance is longer than the signal wavelength, the transmitting signal is carried by an electromagnetic wave, as shown in Fig. 2(a). An electromagnetic wave is used for long-distance transmission. However, the permeability is inferior to electromagnetic coupling transmission. In addition, the antenna size depends on the wavelength, so a higher frequency is required to obtain a small-size device.

When the transmission distance is shorter than the signal wavelength, the transmitting signal is carried by electric and

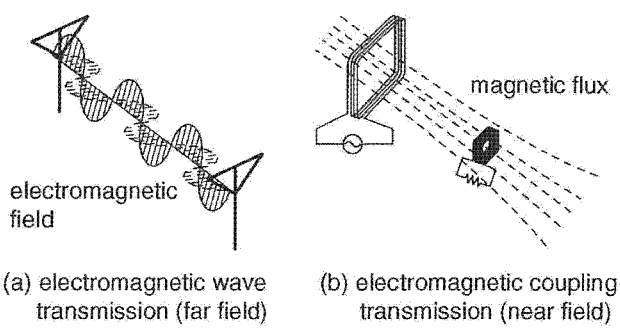


Fig. 2. Electromagnetic wave and electromagnetic coupling transmissions.

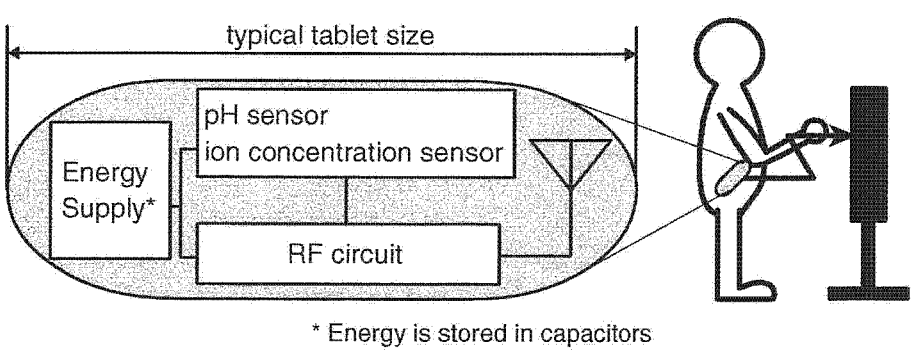


Fig. 1. Schematic of *in vivo* wireless communication chip. It consists of measuring sensors, an RF circuit, an antenna, and an energy supply.

*E-mail address: yama@lsi.pi.titech.ac.jp

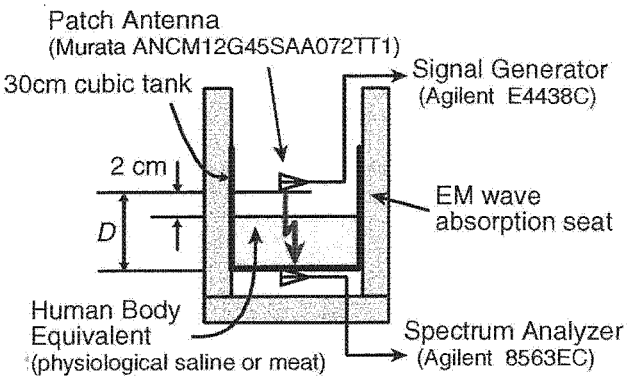


Fig. 3. Measurement setup for far-field transmission.

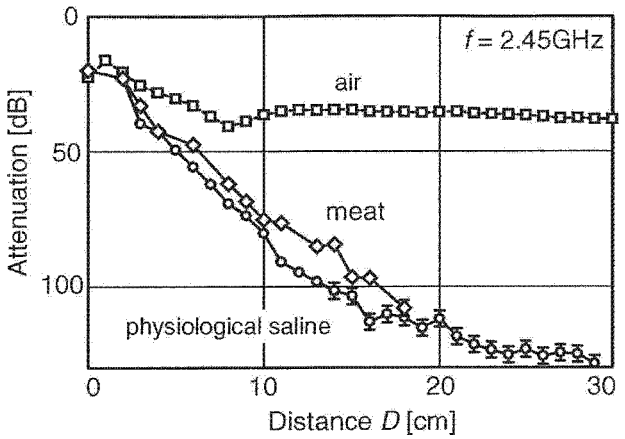


Fig. 4. Attenuation characteristics of far-field transmission through a human body equivalent.

magnetic flux, as shown in Fig. 2(b). Inductive coupling using the magnetic flux is often used in this type of transmission.[2] Inductors are used as antennas, which form a transformer. Inductive coupling transmission cannot transmit over a long distance. Its superior point over electromagnetic wave transmission is its permeability. In addition, the antenna size does not depend on the signal wavelength, so this transmission type is appropriate for a small-size device.

First, we present measured attenuations of far field transmission. Figure 3 shows the measurement setup. A non-modulated sine wave is generated by a signal generator (Agilent E4438C), which is then radiated from a transmitting antenna. The signal frequency is 2.45 GHz, and the signal power is 0 dBm. The transmitted power is measured using a spectrum analyzer (Agilent 8563EC) at the receiving antenna in Fig. 3. Physiological saline and fresh meat are used instead of a real human body.

Figure 4 shows the measured results. The horizontal axis is the thickness of the human body equivalent, and the vertical axis is the measured attenuation. The transmitting antenna is fixed 2 cm above the surface of the human body equivalent. The thickness of a typical human body is 10–20 cm, so the attenuation is 60–90 dB under this condition. From this result, it has too large attenuation to realize the proposed system.

Next, we present measured attenuations of near-field transmission. Figure 5 shows the measurement setup. In conventional measurement, a circular coil is used as the transmitting antenna.[5] In contrast, we use two coils located opposite each other as shown in Fig. 5. Most of the magnetic flux is vertical to these two coils.

A non-modulated sine wave is generated by the signal generator (Agilent E4438C), and a magnetic field is induced by the transmitting coil. The human body equivalent is positioned between the transmitting and receiving coils. A power meter (Agilent E4419B) is used to measure receiving power at the receiving coil, and the attenuation is derived from transmitting and receiving power values. The measurement frequencies are 300 kHz, 1.0 MHz, 3.5 MHz, 13.5 MHz, and 35 MHz. The receiving circuit uses an LC parallel resonant circuit, as listed in Table. I.

Figure 6 shows the measured attenuation for the electro-

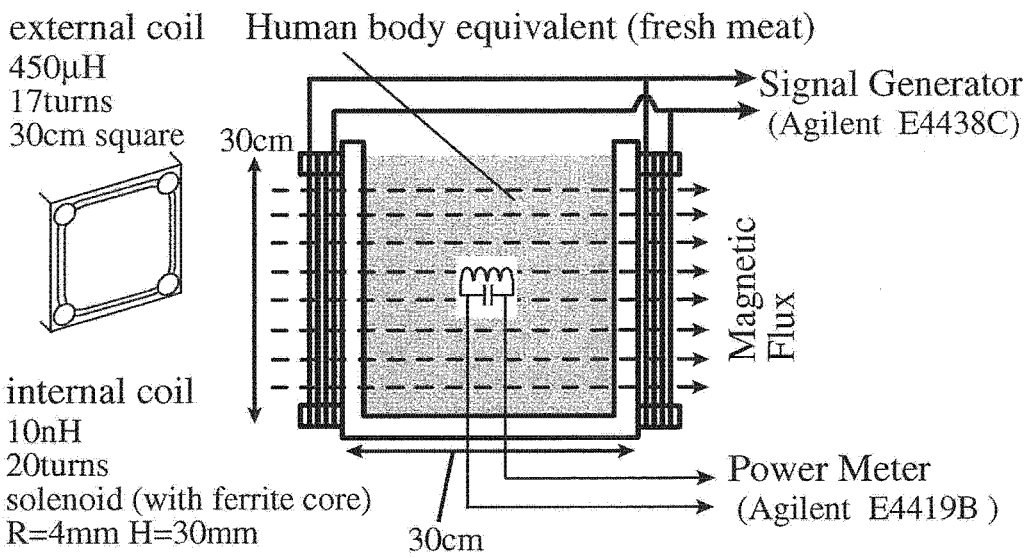


Fig. 5. Measurement setup for near-field transmission.

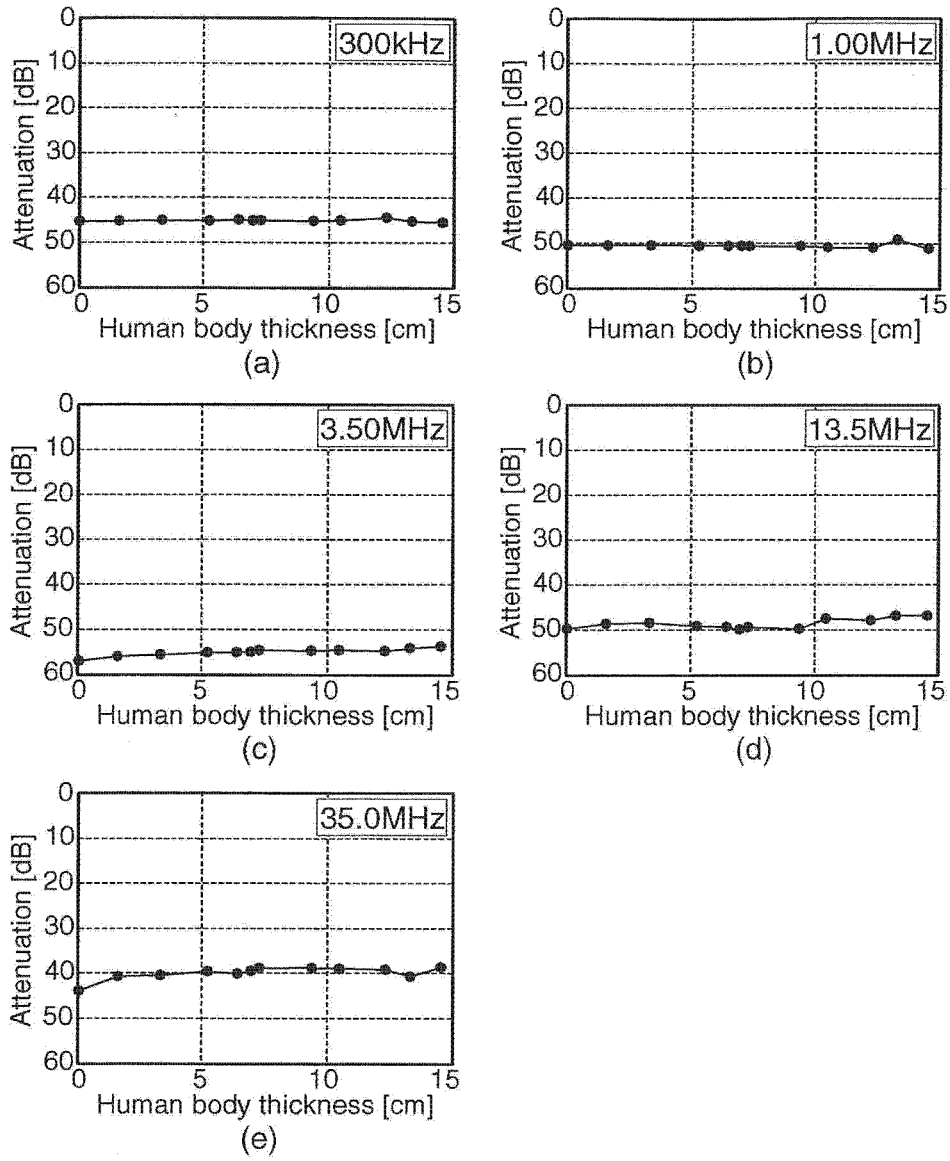


Fig. 6. Attenuation characteristics of near-field transmission through a human body equivalent.

Table I. LC parameters at each resonant frequency.

| Frequency | 300 kHz | 1.0 MHz | 3.5 MHz | 13.5 MHz | 35 MHz |
|---|---|---|---|---|---|
| Inductance | 10 nH | 10 nH | 10 nH | 10 nH | 10 nH |
| Capacitance | 28 μF | 2.5 μF | 200 pF | 14 pF | 2 pF |

magnetic coupling transmission. The horizontal axis is the thickness of the human body equivalent, and the vertical axis is the measured attenuation. We measure every 1 cm thickness of the human body equivalent. The transmitting power is 15 dBm, and the receiving coil is fixed in the center of the tank. The measured attenuations of inductive coupling transmission are lower than those of the 2.45 GHz far-field transmission. The attenuations in Fig. 6 do not have very large differences, and the attenuations are sufficiently small to be used in our proposed system.[3] The frequency of 13.56 MHz is an ISM band. Therefore, we found that the inductive coupling transmission at 13.56 MHz has good feasibility for the proposed wireless communication system.[6,7]

**Acknowledgment**

This work was partially supported by VDEC in collaboration with Cadence Design Systems, Inc.

1) G. Iddan, G. Meron, A. Glukhovsky and P. Swain: Nature **405** (2000) 417.
2) S. Renard, C. Pisella, J. Collet, F. Perruchot, C. Kergueris, Ph. Destrez, P. Rey, N. Delorme and E. Dallard: Proc. 1st Annu. Int. IEEE-EMBS Special Topic Conf. Microtechnologies in Medicine and Biology, 2000, p. 175.
3) K. Okada, T. Yamada, T. Uezono, K. Masu, A. Oki and Y. Horiike: Ext. Abstr. Int. Conf. Solid State Devices and Materials, 2004, p. 366.
4) A. Oki, Y. Takamura, T. Fukasawa, H. Ogawa, Y. Ito, T. Ichiki and Y. Horiike: IEICE Trans. Electron. **E84-C** (2001) 1801.
5) K. Schuylenbergh and R. Puers: Proc. 8th Int. Conf. Solid-State Sensors and Actuators, 1995, p. 55.
6) T. Yamada, H. Uesugi, K. Okada, K. Masu, A. Oki and Y. Horiike: Ext. Abstr. Int. Conf. Solid State Devices and Materials, 2003, p. 366.
7) T. Yamada, H. Sugawara, K. Okada, K. Masu, A. Oki and Y. Horiike: Proc. IEEE Top. Meet. Silicon Monolithic Integrated Circuits in RF Systems, 2004, p. 322.

Japanese Journal of Applied Physics
Vol. 44, No. 4B, 2005, pp. 2879–2882



# *In Vivo* Batteryless Wireless Communication System for Bio-MEMS Sensors

Tomohiro YAMADA, Takumi UEZONO, Kenichi OKADA*, Kazuya MASU†, Akio OKI[1] and Yasuhiro HORIIKE[1]

*Precision and Intelligence Laboratory, Tokyo Institute of Technology, 4259-R2-17 Nagatsuta, Midori-ku, Yokohama 226-8503, Japan*
[1]*Biomaterials Center, National Institute for Materials Science, 1-1 Namiki, Tsukuba, Ibaraki 305-0044, Japan*

(Received October 1, 2004; accepted December 24, 2004; published April 21, 2005)

We propose a batteryless wireless communication system for *in vivo* healthcare chips. The system uses inductive coupling at 13.56 MHz with internal and external coils, and employs pulse interval modulation (PIM) to endure the large attenuation in the human body. A wireless communication circuit is presented in this paper, and 16 mV of output voltage can be obtained at the external receiver. The antenna coil structure is investigated, and it is found that a tablet structure is suitable for the proposed system. [DOI: 10.1143/JJAP.44.2879]

KEYWORDS: wireless communication, batteryless system, communication circuit, *in vivo* chip, healthcare

## 1. Introduction

Biosensors have been developed using bio-MEMS (microelectromechanical system) technology as a key device of $\mu$-TASs (micro-Total Analytical Systems).[1)] In this paper, we propose an *in vivo* wireless communication system to extend the applications of $\mu$-TAS. The proposed system enables small-equipment and batteryless wireless communication through the human body, as shown in Fig. 1. It was implemented on a 1.8-mm-square chip, and it can realize interactive sensing of any portion of the human body either by swallowing or implanting the device into the human body.

The wireless capsule endoscope has been developed as a substitute for the gastric camera.[2)] However, it is too large to swallow and requires a battery. Batteries are usually harmful to the human body. Therefore, small and batteryless system are required. To eliminate the battery, the power consumption of the circuit and the transmitting power must be small. The size of the capsule can also be reduced in the batteryless system. However, the crucial problem of *in vivo* wireless communication is the very large attenuation in the human body, and this attenuation is often varied by movements of the human body. We investigate the circuit architecture, communication algorithm, and modulation for the small, low-power and batteryless wireless communication system.

Section 2 describes the carrier frequency and modulation. The designed communication circuit is explained in §3, and the antenna coil structures are investigated in §4.

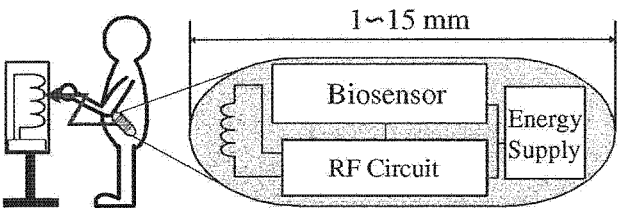


Fig. 1. Schematic of *in vivo* wireless communication chip, which consists of measuring sensors, RF circuit, antenna, and energy supply.

*E-mail address: okada@pi.titech.ac.jp
†E-mail address: masu@pi.titech.ac.jp

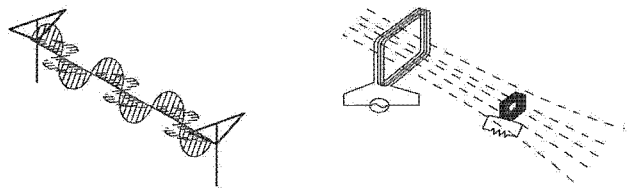


Fig. 2. Transmission types: (a) electromagnetic wave transmission (far-field communication) and (b) inductive coupling transmission (near-field communication).

## 2. Carrier Frequency and Modulation

### 2.1 *Carrier frequency*

Figure 2 shows the transmission types of the electromagnetic wave and electromagnetic coupling. When the transmission distance is longer than the signal wavelength (far-field communication), the transmitted signal is carried by an electromagnetic wave. On the other hand, when the transmission distance is shorter than the signal wavelength (near-field communication), the transmitted signal is carried by the electric and magnetic fluxes. With regard to permeation characteristics, electromagnetic coupling transmission has the advantage over electromagnetic wave transmission.

Attenuation characteristics through the equivalent of a 15-cm-thick section of the human body are measured at 2.45 GHz,[3)] and then transmitted as an electromagnetic wave. We also measure the attenuation characteristics at 300 kHz, 1 MHz, 3.5 MHz, 13.56 MHz, and 35 MHz.[4)] At these frequencies, a signal is transmitted by near-field communication. We therefore use 13.56 MHz for the proposed system because it is an Industrial Science Medical band (ISM band) and we can employ electromagnetic coupling transmission. Although 300 kHz also exhibits small attenuation, it is not an ISM band. Therefore, 13.56 MHz is suitable for the proposed system.

### 2.2 *Modulation*

We propose the use of pulse interval modulation (PIM) in the *in vivo* wireless communication system.[4)] Table I shows a comparison between amplitude shift keying (ASK), frequency shift keying (FSK), phase shift keying (PSK),

Table I. Comparison of modulations.

| Modulation | ASK(AM) | FSK,PSK(FM) | PIM |
|---|---|---|---|
| Attenuation robustness | fair | good | good |
| Power consumption | good | fair | good |
| Bit rate | good | good | fair |

and PIM. It is difficult to use conventional modulations, because the attenuation is often varied by movements of the human body, and power consumption must be reduced to as low as possible. ASK is considerably affected by the fluctuation of attenuation. FSK and PSK require circuits such as an oscillator, an amplifier, and a mixer, which consume much power. For data transmission, PIM uses two pulse signals, and data are represented by the time interval between two pulse signals. Therefore, data transmission is not affected by the attenuation in the human body. An oscillating circuit is also unnecessary for PIM, so power consumption can be reduced. Therefore, PIM at 13.56 MHz is suitable for the proposed system.

## 3. Communication Circuit

The S/N ratio is an important issue for batteryless wireless communication, so the transmitting sequence is separated into two phases. In the first phase, an internal device is charged up by inductive coupling from an external coil to an internal coil, and the measuring sensor measures medical information of the internal body. In the second phase, the internal device transmits the medical information to the external coil. At this time, charging from the external coil is halted to avoid insensitive. Figure 3 shows the block diagram of the designed system. The symbol $k$ represents the coupling factor.[4)]

### *3.1 Voltage booster circuit*

Figure 4 shows a voltage booster circuit. The induced electromotive force depends on the coupling factor between the external and internal coils and is usually not very high. This circuit provides six times as high a voltage as the input voltage. At the output of this circuit, the maximum voltage is limited by a limiter circuit below 4.0 volts. It consists of several diodes.

### *3.2 PIM circuit*

Figure 5 shows a PIM circuit and two capacitors for the power supply. PIM needs two pulses, so two capacitors are required as a pulse source. During the first phase of the

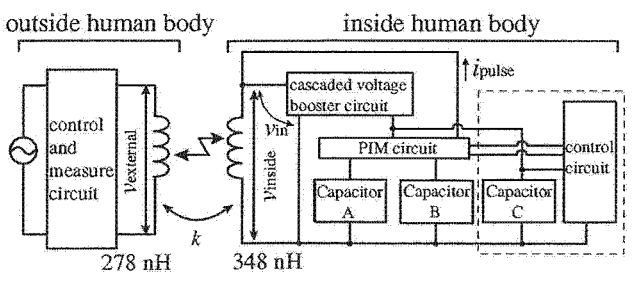


Fig. 3. Block diagram of wireless communication circuit.

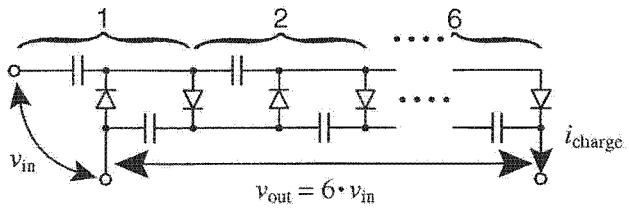


Fig. 4. Voltage booster circuit consisting of 12 diodes and 12 small capacitors. All diodes are PN junction diodes.

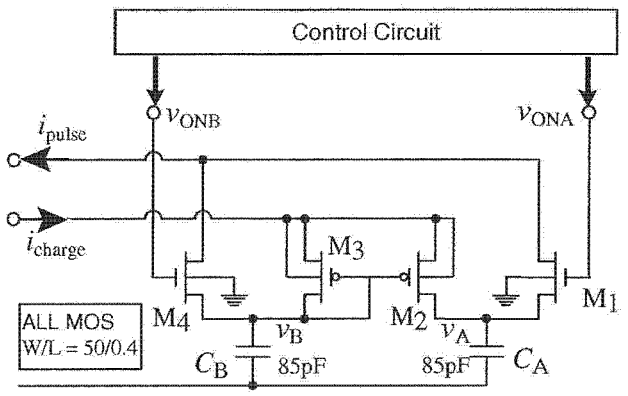


Fig. 5. PIM circuit and capacitors.

communication, capacitors A and B are charged up through transistors $M_2$ and $M_3$ by current $i_{charge}$ from the voltage booster circuit. At this phase, transistors $M_1$ and $M_4$ are turned off. When both capacitors are charged, transistors $M_2$ and $M_3$ are turned off by the control signal $v_B$. During the second phase, the control circuit turns on the control signals $v_{ONA}$ and $v_{ONB}$. For the first pulse, transistor $M_1$ is turned on by $v_{ONA}$, and a pulse current is generated from capacitor A until voltage $v_A$ becomes low. However, capacitor B does not discharge at this time, because transistors $M_2$ and $M_3$ remain off. For the second pulse, transistor $M_4$ is turned on by $v_{ONB}$, and pulse current is generated from capacitor B until voltage $v_B$ becomes low. When $v_B$ becomes low, transistors $M_2$ and $M_3$ are turned on, and capacitors A and B discharge completely.

### *3.3 Simulation results*

Figures 6, 7 and 8 show the time-domain simulation results of the proposed system at $k = 0.5$. Figure 6 shows the capacitor voltage during charging time. During the first phase, the capacitor is charged by the external coil. Figure 8 shows the voltage at the external coil. During the second phase, the time interval between the first and the second pulses is determined according to the measured medical information. The coupling factor, which is used in these simulations, is not very large for the proposed system. When the coupling factor is small, the induced voltage at the internal coil also decreases. In this case, if we provide a large voltage to the external coil, the capacitors in the internal circuit can be fully charged. On the other hand, the small coupling factor also causes the reduction of the output pulse amplitude at the external coil. Table II shows the simulated peak-to-peak voltage of the first pulse as a function of the

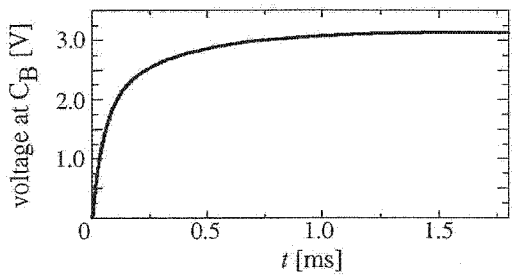


Fig. 6. Simulated voltage at the capacitor $C_B$ at $k = 0.5$.

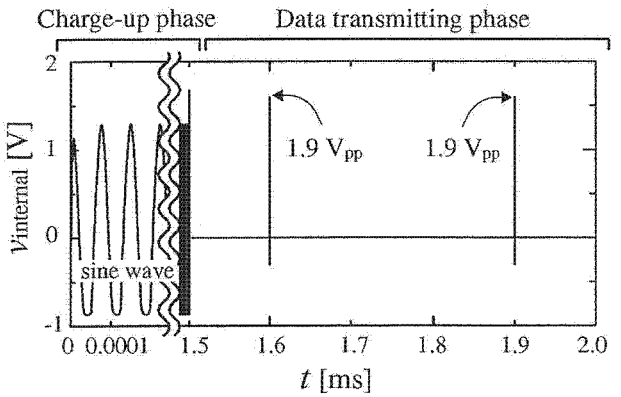


Fig. 7. Simulated voltage at the internal coil at $k = 0.5$.

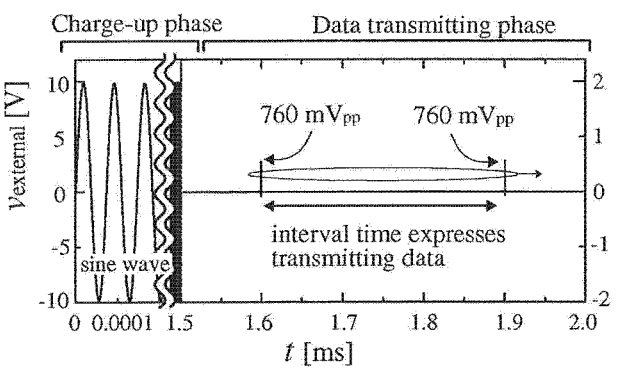


Fig. 8. Simulated voltage at the external coil at $k = 0.5$.

Table II. Simulated peak-to-peak voltage of the first pulse.

| Coupling factor $k$ | 0.1 | 0.2 | 0.5 | 1.0 |
|---|---|---|---|---|
| $v_{external\ pp}$ | 16 mV | 340 mV | 760 mV | 2.3 V |

coupling factor $k$. Figure 9 shows the simulated result for the PIM circuit shown in Fig. 5. The pulses are generated by the capacitors when the control signal turns on.

Figure 10 shows the designed layout using a 0.35 μm Si CMOS process, with the core size of 1.8 mm square. At this time, we implemented the proposed system without the control circuit.

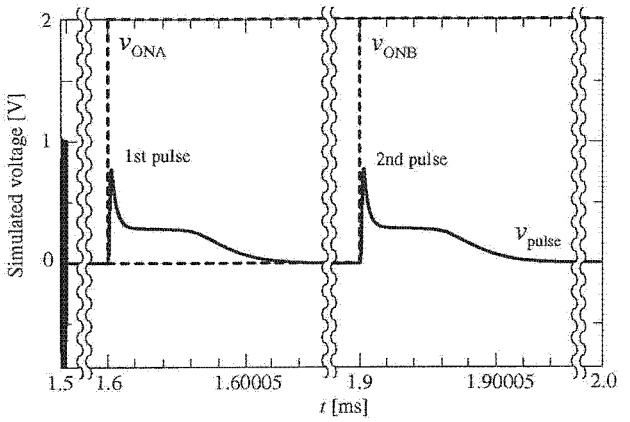


Fig. 9. Simulated pulse signal generated by PIM circuit shown in Fig. 5.

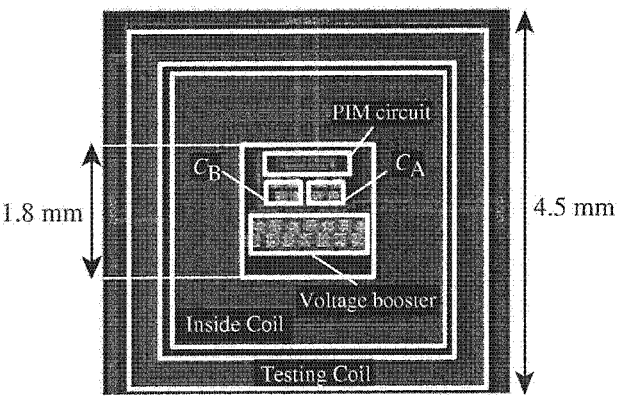


Fig. 10. Layout of TEG.

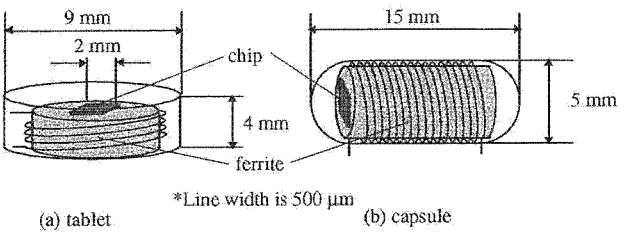


Fig. 11. Antenna structures.

## 4. Antenna Coil Structure

From the result of Table II, to improve the S/N ratio, the coupling factor $k$ should be large. We hence investigate the coupling factor between the external and internal coils. Figure 11(a) shows a tablet structure; the size is 4.5 mm in diameter and 4 mm in height. Figure 11(b) shows a capsule structure; the size is 2.5 mm in diameter and 15 mm in length. Both sizes are common in usual medicines. The magnetic flux density at the center of the external coil is given by the Biot-Savart law:

$$B = (\mu I/\pi r) \cdot N_1 \cdot 2, \quad (1)$$

where $\mu$ is the permeability, $I$ is the current of the external coil, $r$ is the radius, and $N_1$ is the number of turns in the external coil. The mutual inductance is calculated by

Table III. Calculated parameters for each antenna structure in Fig. 11.

| Core | Without ferrite core | | With ferrite core | |
|---|---|---|---|---|
| Structure | tablet | capsule | tablet | capsule |
| Self inductance | 304 nH | 343 nH | 142 μH | 243 μH |
| Coupling factor $k$ | 0.0032 | 0.0019 | 0.095 | 0.066 |
| $v_{\text{external pp}}$ | 120 mV | 75 mV | 230 mV | 125 mV |

$$M = \sum_{a=0}^{N_2} B \cdot S_a, \tag{2}$$

where $S_a$ is the internal coil area at the $a$-th turn, and $N_2$ is the number of turns in the internal coil. The coupling factor is calculated by

$$k = M/\sqrt{L_1 \cdot L_2}, \tag{3}$$

where $L_1$ is the self-inductance of the external coil, and $L_2$ is the self-inductance of the internal coil.

Table III shows the calculated result of the coupling factor and the simulated result of peak-to-peak $v_{\text{external}}$. The coupling factor is calculated in both structures with or without a ferrite core under the same outer shapes. If the ferrite core is not used, the empty space in the tablet and capsule can be used for coil lines in place of the ferrite core. In this result, the tablet structure is suitable for the proposed system, and the coupling factor with ferrite is better than that without ferrite.

## 5. Conclusions

We proposed a batteryless wireless communication system capable of transmitting data through the human body. The proposed system uses PIM at the 13.56 MHz band because (1) the attenuation through the human body is not appreciably large at 13.56 MHz, (2) 13.56 MHz is an ISM band, (3) PIM is not affected by dynamic changes of the attenuation, and (4) the power consumption of PIM is low. We described the communication circuit and antenna coil structure. The data in the proposed circuit can be transmitted as two pulses, and the results show that a tablet structure is suitable for the proposed system.

## Acknowledgment

This work was partially supported by MEXT.KAKENHI and JSPS.KAKENHI from the Japanese government, and VDEC in collaboration with Cadence Design Systems, Inc.

1) A. Oki, Y. Takamura, T. Fukasawa, H. Ogawa, Y. Ito, T. Ichiki and Y. Horiike: IEICE Trans. Electron. **E84-C-12** (2001) 1801.
2) G. Iddan, G. Meron, A. Glukhovsky and P. Swain: Nature **405** (2000) 417.
3) T. Yamada, H. Uesugi, K. Okada, K. Masu, H. Nakase, K. Tsubouchi, A. Oki and Y. Horiike: *Ext. Abstr. Int. Conf. Solid State Devices and Materials* (2003) p. 366.
4) T. Yamada, T. Sugawara, K. Okada and K. Masu: *Proc. IEEE Workshop on Wireless Circuits and Systems* (2004) p. 31.

Japanese Journal of Applied Physics
Vol. 45, No. 5A, 2006, pp. 4241–4247



# Healthcare Chip Based on Integrated Electrochemical Sensors Used for Clinical Diagnostics of Bun

Chia-Hsien CHANG*, Hiroki OGAWA[1], Akio OKI, Madoka TAKAI[2], Masao NAGAI[1], Hideaki HISAMOTO[3] and Yasuhiro HORIIKE

*National Institute for Materials Science, 1-1 Namiki, Tsukuba, Ibaraki 305-0044, Japan*
[1]*Adbic In. Corp., 2-1-6 Sengen, Tsukuba, Ibaraki 305-0047, Japan*
[2]*Department of Materials Engineering, University of Tokyo, 7-3-1 Hongo, Bunkyo-ku, Tokyo 113-8656, Japan*
[3]*Graduate School of Material Science, University of Hyogo, 3-2-1 Kouto, Kamigouri, Akou-gun, Hyogo 678-1297, Japan*

(Received December 28, 2005; accepted February 11, 2006; published online May 9, 2006)

Research based on health marker sensors, such as $Na^+$, glucose, $K^+$ have been carried out using integrated ISE (ion selectivity electrode). In this study, focus has been placed on potentiometric measurement of ammonia and blood urea nitrogen (BUN) sensors using new 19-membered crown ionophore, TD19C6 (2,6,13,16,23,26-hexaoxaheptacyclo-[25.4.4.4 7,12.4 17,22.O 1,17.O 7,12.O 17.22]), poly(vinyl chloride) (PVC) membranes along with anionic additives, potassium tetrakis(4-chlorophenyl)borate (k-TCPB), sodium tetrakis(4-fluorophenyl)borate dehydrate (TFPB), and plasticizers, bis(1-butylphenyl)adipate (BBPA) and tris(2-ethylhexyl)trimellitate (TOTM). Screen-printed electrodes Ag/AgCl (250 mm in diameter) and a disposable polycarbonate chip (PC) designed using a trace amount of whole blood are also used.
[DOI: 10.1143/JJAP.45.4241]

KEYWORDS: healthcare chip, BUN, clinical diagnostics, $\mu$-TAS, screen printed electrode, TD19C6

## 1. Introduction

In biosensor development, the concept of a micro-total analytical system ($\mu$-TAS) and a lab-on-a-chip system[1–3] has emerged as a means of providing vital technology to enable medical self-check-up at home. Nowadays, it is generally believed that in most developed countries, such as Japan, UK, USA, and EU, owing to the increasing number of elderly in our society; medical costs have become a burden to their governments. To reduce the medical cost it would be helpful to develop a miniaturized diagnostic device, which is highly sensitive, quick response time, inexpensive, disposable and convenient for everyone to use.

As known in the field of clinical chemistry, various health markers such as $Na^+$, $K^+$, glucose, blood urea nitrogen (BUN), creatine and creatinine have been used to indicate an individual's health condition and can be used to screen some life-threatening diseases, for example kidney-related diseases or hepatic function failure. In our research group, the possibility of developing solid-state sensors with an integrated miniaturized device has been investigated[4–7] along with several key techniques required to enhance diagnostic processes.[8] These range from painless needles, made of stainless (SUS) tubes 150 µm in diameter with an 80 µm bore, the surface of which is hardened using plasma nitrification and the inner wall of which is electrochemically polished in a phosphoric acid solution; these needles are used to complete the first step of extracting blood. Secondly, in electronical blood collection, the blood vessel is visualized using an array of near-infrared (NIR) light emitting diodes with a wavelength of 850 nm, the potential change against elapsed time in seconds shown is used to detect the depth of vessel and all these operations can be performed by only focusing on a computer display without actually observing the blood vessel in the arms. Thirdly, new screen-printed carbon and KCl-saturated Ag/AgCl reference electrodes coated on carbon-silver wires have also been developed (Fig. 1). Finally, the screen-printed electrode is then attached to an injection molded polycarbonate plate with a channel pattern (Fig. 1) assembled with a painless needle to complete the healthcare chip. In accordance with the channel design, the operation of the healthcare chip is solely carried out using centrifugal force. As a result, 6 µl of blood is collected using the painless needle and the blood is centrifuged in one direction to obtain plasma and carry out potentiometric measurement later. After measuring, the chip is rotated 90 deg and centrifuged to discard the waste. The cost of the chip design is kept low as it is, only used once and is disposable.

In the previous study,[8] it was shown that BUN measurement is based on the detection of proton loss [$H^+$] during the reaction, $NH_2CONH_2$ (urea) + $2H_2$ + $H^+$ → $NH_4$ + $HCO_3^-$, in the presence of urease. However, in human blood or serum, occasionally a slight change pH in body chemistry might give rise to interference during measurement and cause unstable and inaccurate measurement. To

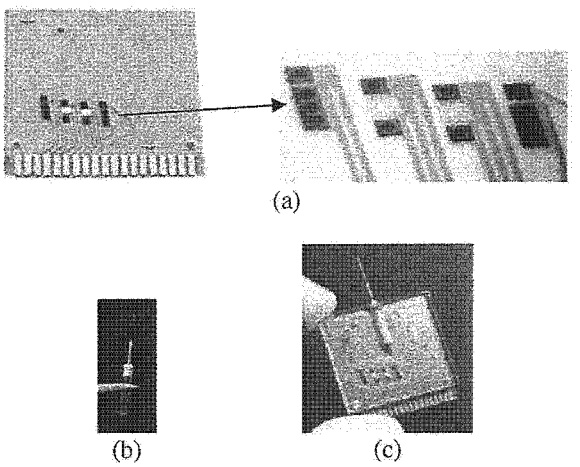


Fig. 1. (a) Screen-printed Ag/AgCl electrode, (b) painless needle, (c) injection molded micro-fluidic channel plate (27 × 24 × 1.5 mm³).

*E-mail address: CHANG.chiahsien@nims.go.jp

avoid this problem, we have adopted another method, which is based on the detection of ammonia ions using an ionophore-based poly(vinyl chloride) (PVC) membrane covered with a catalytic urease enzyme layer which in turn is covered by solvent-casting hydrophilic cellulose acetate polymer. As we know, urease is an enzyme that carries out hydrolysis of urea and turns urea into ammonia and carbon dioxide. The reaction is $NH_2CONH_2$ (urea) $+ 2H_2O \rightarrow 2NH_4^+ + CO_3^{-2}$ in the presence of urease and water. The released ammonia ions from hydrolysis are then detected by the ion-selective ionophore membrane measuring the potential difference between different concentrations of ammonia solutions. Consequently, the detected potential from various concentrations may have to fit the calculated results through the Nernst equation.

The design of the healthcare chip is used *in vitro* quantification of various specific analytes, such as BUN/urea in arterial, venous or capillary whole blood. As known in the clinical chemistry, the average concentration of urea nitrogen/BUN and urea in normal humans may vary from person to person and depends largely on his/her body chemistry. According to the reported values, the reference range of urea nitrogen/BUN is from 8 to 26 mg/dl (to convert a BUN result in mg/dL to a urea result in mmol/L, multiply the BUN result by 0.357). As a result, to be able to detect the urea or BUN, a detection limit of 1 mM is essential. In this study, we demonstrate successful measurement of BUN at a level of 1 mM.

One of the most important issues in developing a healthcare chip is the design of the reference electrode. It has to meet in several criteria, for example quick response time, long life time and not be contaminated and affected during measurement. Generally, there are two types of reference electrodes existing, one is a liquid-based reference electrode filled with saturated potassium chloride or sodium chloride and the other is a nonliquid-junction type reference electrode. Conventional liquid-based reference electrodes are made of Ag/AgCl wires sealed with a glass tube and porous ceramics at the bottom to create an ironically conducting electrical pathway between the inside of the reference electrode and the bulk of the measuring cell. Normally the tube is filled with saturated potassium chloride, sodium chloride and in some special cases LiCl is used. As saturated solutions of KCl or NaCl are used for filling solutions it has the advantage that the concentration is reproducible even if the temperature changes (if solid salt is present) and is not influenced by the effects of water evaporation. However, the solid salt hardens into an impenetrable block, which may lead to a high impedance electrode. In some cases, a solution of less saturated solutions such as 3.5 M KCl or 3 M NaCl are used but the concentration can be changed due to evaporation, in which might cause instability during the measurement. In this study, the high concentrations of KCl and NaCl might give rise to interference during the measurement, particularly when the target solution's concentration is low. To be able to reduce interference, a double-junction reference electrode filled with 0.3 M $NH_4NO_3$ in a tube covering the standard reference electrode is used throughout the whole study. In this publication, we also demonstrate a nonliquid-junction type reference electrode. The electrode is constructed on a sputter-deposited Ag surface chlorinated with chemical solutions (such as $FeCl_3$, or a mixture of $K_2Cr_2O_7$ with HCl) as a base Ag/AgCl layer on silicon and coated with a PVC membrane to improve the sensitivity and durability of the solid-state reference electrode. Test results show a quick response time, a long life time and unlikelihood of being contaminated by target solutions.

## 2. Experimental Procedure

### *2.1 Reagents and materials*

PVC of high molecular weight was purchased from Wako, Japan Chemicals, the plasticizers BBPA bis(1-butylphenyl)adipate and TOTM tris(2-ethylhexyl)trimellitate from Fluka, the anionic additives K-TCPB potassium tetrakis-(4-chlorophenyl)borate, TFPB, sodium tetrakis(4-fluorophenyl)borate dihydrate from Fluka, ammonia ionophore 2,6,3,6,23,26-hexaoxaheptacyclo-[25.4.4.4 7,12.4 17,22.O 1,17.O 7,12.O 17.22] TD19C6, DOJINDO, tetrahydrofuran (THF) from Wako, urease lyophilized powder from jack bean, Sigma, and cellulose acetate from Wako Chemicals; fresh $NH_4Cl$ (1 M) stock solutions were prepared. Dilution to appropriate concentration was preformed just before direct and calibration measurements. All aqueous solutions were prepared in double deionized water (18.2 MΩ·cm$^{-1}$, 25 °C).

### *2.2 Ion selective membrane*

The solvent polymeric membranes were prepared with a mixture of ionophore 3 wt % TD19C6, 67 wt % plasticizers BBPA or 67 wt % TOTM, 30 wt % PVC and anionic additives K-TCPB or 10 mol % TFPB. Firstly, PVC was gradually dissolved in 2 ml THF with a sonic shaker for two hours, followed by the addition of anionic additives, ionophore (dissolved in 1 ml of THF) and finally plasticizer. The cocktail of the PVC-based sensor membranes was fabricated using an auto dispenser or manual dispenser.

### *2.3 Enzyme immobilization*

Lyophilized urease powder from jack bean, 2660 units/ml, were dissolved in a solution of 0.1 M Tris/HCl, 5 wt % glycerol and 0.01 M ethylenediaminetetraacetic acid (EDTA) and kept at 4 °C before use. The urease was immobilized by the deposition of a cellulose acetate layer with 50 mg/ml acetone. The urease enzyme activity was tested using the following methods and chemicals provided by Wako Pure Chemical Industries, Ltd.

### *2.4 Measurement of ammonia and BUN sensors*

Electrode response potential (EMF) measurements were performed at room temperature (20 °C), data were recorded using Labview software under stopped-flow conditions. Sensors were measured in various $NH_4Cl$ concentrations (ranging from 1 mM, 0.01 M, 0.1 M to 1 M). Screening of the electrodes was carried out by determining the slope of the calibration curve (potential versus time/s). There was no preconditioning before carrying out ammonia measurement, however, preconditioning of 0.1 M urea for 2 h before BUN measurement was considered necessary in this study. The reference electrode used during the measurement was a double-junction electrode containing an inner KCl saturated calomel electrode with an outer solution of 0.3 M $NH_4NO_3$.

Table I. Different recipes used for the sensing membrane.

| | Plasticizers (67 wt %) | | Anionic additives (10 mol %) | | (3 wt %) | (30 wt %) |
|---|---|---|---|---|---|---|
| | BBPA | TOTM | K-TCPB | TFPB | TD19C6 | PVC |
| Formula 1 | * | | * | | * | * |
| Formula 2 | * | | | * | * | * |
| Formula 3 | | * | * | | * | * |
| Formula 4 | | * | | * | * | * |

*Components contained in the ion-selective membrane.

*2.5 Fabrication of non-liquid junction reference electrode*

Processes of fabricating non-liquid junction reference electrode are as follows. (1) A 2 μm polyimide film was spin-coated at a speed of 4000 rpm on an 800 nm Ag/50 nm Cr film which was sputter-deposited using a Ni film stencil mask on a 1 μm $SiO_2$/Si substrate. (2) A hole 100 μm in diameter was opened in the polyimide film with NMD-3 solution (2.38%, TOK, Japan) and clean-washed using IPA solvent. (3) The Ag film was chlorinated to become AgCl base layer by treatment of 0.5 M $FeCl_3$ solution, forming the Ag/AgCl electrode. (4) A ring-like well 50 μm in height with a 700 μm bore was fabricated using an SU-8 photoresist (MicroChem Corp.) (5) 20 nL of 2.5 wt % poly vinyl alcohol (PVA; number average degree of polymerization: $n = 500$, WAKO) + 0.5 M potassium chloride (KCl) solution were dispensed on the Ag/AgCl electrode and then dried on a hot plate at 100 °C. (6) 1 : 1 weight ratio of PVC ($n = 1100$, WAKO) and dioctyl sebacate (DOS; WAKO) were dissolved in tetrahydrofuran (THF) (solid content: 15 wt %) and deposited to cover the surface area.

## 3. Results and Discussion

*3.1 Ammonia membrane formation and composition*

To recognize ammonia ions selectively, ammonia ionophore, a 19-membered crown ether derivative (TD19C6) is used. Previously, it was reported that to measure ammonia ions from testing solution, the introduction of an ether cyclic structure in a compound is useful and owing to the similar ionic size of ammonia ion and potassium ion, a molecular design of introducing a rigid frame and "block-walls" is necessary to prevent the formation of both a wrapping complex of the crown ether with a smaller ion and a sandwich complex with a larger ion.[9,10] On the other hand, considering the hydrogen bonding distance of $K^+$···O and NH···O, the latter bonding is slightly larger. As a result, $NH_4^+$ has a larger ionic size than that of $K^+$. In the designation of TD19C6, the size of crown ether using 19-crown-6 is larger than that using 18-crown-6, which is conventionally used for measuring $K^+$ ions. In addition, in accordance with the previous report, TD19C6 has a high $NH_4^+$ selectivity over $K^+$ ($\log K^{pot}_{NH_4^+,K^+} = -1.5$) and $Na^+$ ($\log K^{pot}_{NH_4^+,Na^+} = -2.5$). In our study, the membrane consists of two types of plasticizers, BBPA and TOTM, in combination with two anionic additives, K-TCPB and TFPB, along with ammonia ionophore, TD19C6, matrix material, PVC and all components are dissolved in THF solvent. During the study, the proportions of plasticizers, anionic additives, ammonia recognizable ionophore, and PVC contents in the membrane are important and have been investigated; the most suitable proportions are listed in Table I. In our study, PVC and two plasticizers have been selected due to their cost, easy handling and accessibility. In the membrane, PVC acts as a matrix and plasticizers as cross linkers to physically immobilize TD19C6 and anionic additives. Two different plasticizers, BBPA and TOTM are used to investigate whether the linear chemical structure of BBPA has higher cross-linking properties in comparison with the 3-dimensional structure of TOTM plasticizer with naturally blocking properties. As for the two types of anionic additive used, differences between two compounds are TFPB with four fluorine atoms attached to four benzene rings forming borate complexes with sodium ions and K-TCPB with chlorine atoms bonded to four benzene rings in borate complexes with potassium ions. As a result, two anionic additive compounds significantly affect detection. The most important part of this study is the use of TD19C6 to create rigidity of the cyclic compound and introduce blocking efficiency forming a complex with ammonia ions.

The electrode used is a screen-printed electrode, which is constructed with a screen-printed Ag layer followed by a screen-printed AgCl layer, Fig. 1(a). The layers of 0.1 M ammonium chloride in the presence of 0.5% PVP (polyvinylpyrrolidone) and the ammonia-sensing membrane are deposited using an autodispenser owning to the uniform surface characteristics achieved, which is helpful during the measurement (Fig. 3). As shown in Fig. 1(a), the screen-printed AgCl layer is designed to have an open diameter of

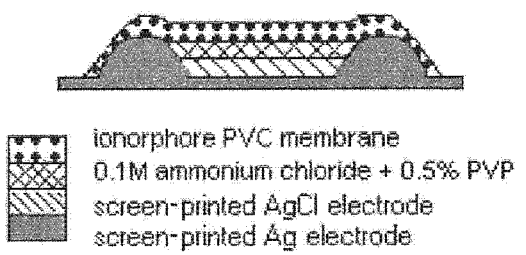


Fig. 2. Sandwich formation of ammonia-sensing membrane and electrode. Note that the AgCl layer is 250 nm in diameter.

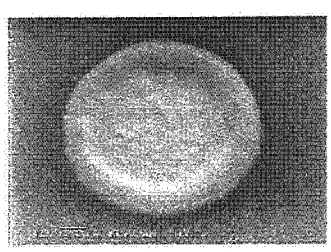

Fig. 3. Image of surface formation of membrane on electrode obtained by SEM (120 × 83.3 μm WD 20.6 mm).

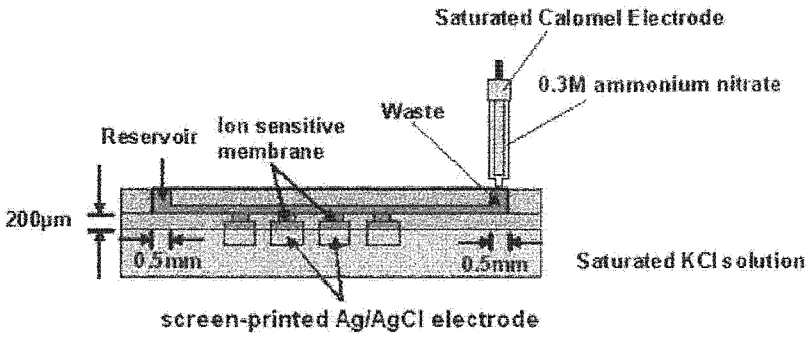


Fig. 4. Measurement setup cross section of a chip fabricated for evaluation of selectivity.

250 nm, which is ideal for use in future miniaturized device purpose. Figure 1(c) shows an injection molded microfluidic system of collecting whole blood using a painless needle [Fig. 1(b)] and of obtaining plasma by applying a centrifugal force. Measurement followed by waste removal can be carried out in one simple chip and most importantly the cost is not high.

### *3.2 Electrode membrane potential (EMF) measurement*

ISE sensors undergo a series of potentiometric tests to meet the requirements for *in vitro* clinical use. As reported in the i-STAT system,[11,12] 100 μL of blood is required for checking various markers. In our study, a new type of chip has been developed in which only 4 μl of blood is necessary to run the analysis. In the case of ammonia sensors, measurements are carried out firstly in an open-field environment followed by closed-field measurement on the chip. Freshly made stock 1 M $NH_4Cl$ solution diluted to 1 mM, 0.01 M and 0.1 M has been used. In this study, a saturated calomel reference electrode and double-junction reference electrode containing 0.3 M $NH_4NO_3$ are used to reduce interferences that might be caused by the leakage of saturated KCl solution from the calomel reference electrode (see setup, Fig. 4). The double-junction configuration design is used to allow saturated KCl solution balancing with $NH_4NO_3$ in the beginning without significantly disturbing the targeting solution.

Recently, BUN sensors based on ion-sensitive field effect transistors (ISFETs) used for detecting pH change have been developed.[13] However, due to some difficulties, the development of BUN has been moved to the ion-selective membrane field. In the history of development, preconditioning of the membrane is still necessary. Using the data obtained during EMF measurement, Fig. 5 shows formulas 1(a) and 2(b) with proper inner layer containing 0.1 M ammonium chloride in the presence of 0.5% PVP can be used to give quick response time and good reliability to detect $NH_4Cl$ ranging from 1 mM, 0.01 M, 0.1 M and 1 M in the range of 50–60 mV in potential decade. In our study, preconditioning is not necessary to detect concentration of 1 mM of ammonia solution. This may be explained by the fact that in some cases, PBS solution or a low concentration target solution are used for preconditioning the ion-selective membrane to increase the detection limit. In the case of hydrophobic membranes being used for membrane matrix, such as PVC, a long preconditioning duration time might be necessary because the resistance of the membrane might have been reduced by rinsing the membrane in the solution before EMF measurement. In the case of hydrophilic membranes being used, a short preconditioning duration time might also be helpful. On the other hand, changing the design of the deposition inner layer might be another way of achieving a low detection limit as well as avoiding preconditioning.

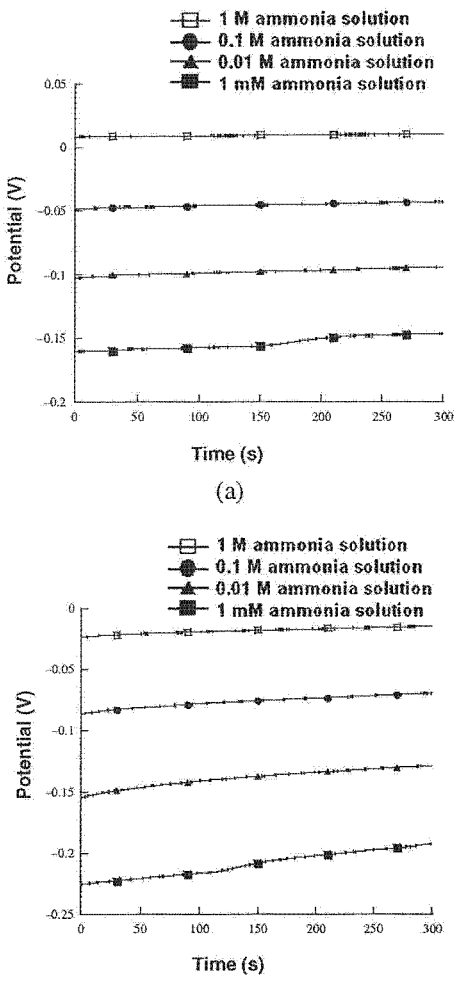


Fig. 5. EMF measurement of formula 1(a) and formula 2(b), showing stable measurement contributed by proper inner layer of 0.1 M $NH_4Cl$ in presence of 0.5% PVP.

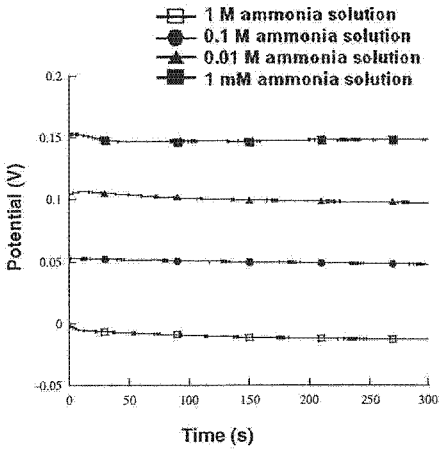


(a)

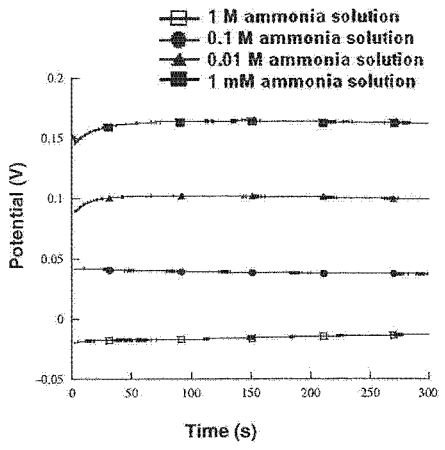


(b)

Fig. 6. EMF measurement of formulas 3(a) and 4(b), showing stable measurement contributed by proper inner layer of 0.1 M $NH_4Cl$ in presence of 0.5% PVP.

In the case of formula 3(a) and formula 4(b), shown in Fig. 6, although most of the membrane components and inner layers are similar to those of formula 1 and formula 2, the concentration of target solutions increase with decreasing EMF. This indicates that the plasticizer BBPA works better than TOTM as a cross-linker with PVC in terms of when the components in the membrane leak out, the EMF values will decrease gradually. The cross-linking between BBPA and PVC seems stable compared with the TOTM membrane. As a result, different anionic additives may provide certain advantages and enhancements to a certain extent. In our study, we observed the difference between two anionic additives which showed that BBPA is better than TOTM. Thus, we use BBPA as a plasticizer throughout the whole study.

### *3.3 BUN sensor*

When measuring urea ions, the ions can diffuse into the membrane and reach an equilibrium on both sides of the membrane. Urea enzymes can then digest urea into ammonia ions and the ammonia-sensing membrane can detect various ammonia concentrations from target solutions. In our study, a sensing electrode composed of membrane layers is used to

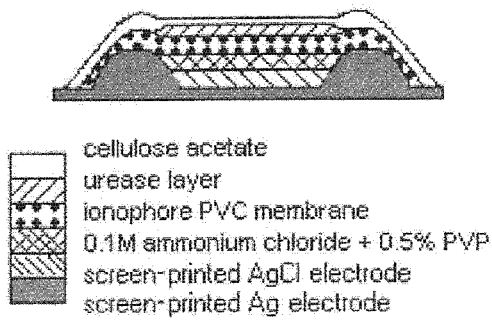


Fig. 7. Sandwich formation of ammonia-sensing membrane and electrode.

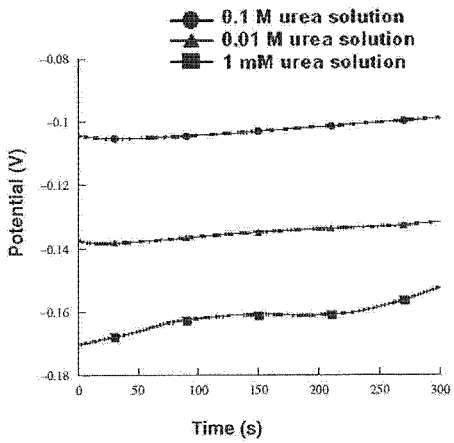


(a)

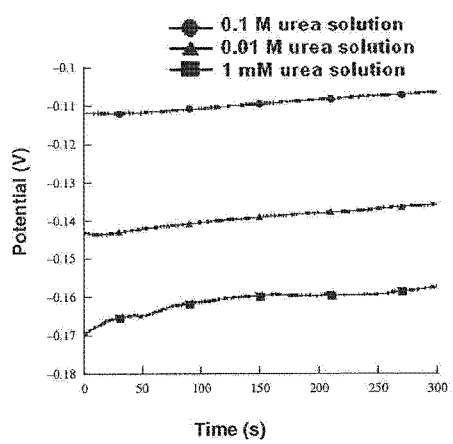


(b)

Fig. 8. EMF measurement of formulas 1(a) and 2(b), showing stable measurement based on measuring ammonia ions using TD19C6 ionophore.

detect various ammonia concentrations. As showed in Fig. 7, a layer of urea enzyme, 2660 units/ml, in the presence of 0.1 M Tris/HCl, 5 wt% glycerol and 0.01 M EDTA is deposited using an autodispenser followed by a solvent casting layer of hydrophilic cellulose acetate layer. The results show stable measurements with various urea concentrations ranging from 1 mM, 0.01 M and 0.1 M to 1 M. In Fig. 8, the potential change per decade is approximately 35 mV of formula 1(a), while in formula 2(b) it

shows reasonable potential change of lower than 35 mV per decade. This indicates that formulas 1 and 2 with proper inner layer anionic additives might provide better detection conditions. In the BUN sensor study, formula 3 and formula 4 are not suitable for detection owing to their low stability to immobilize necessary components inside the membrane and this can be observed as mentioned above.

### *3.4 Nonliquid-junction type reference electrode*

A reference electrode, which generates a standard potential, is important for pontentiometric electrochemical biosensors, regardless of the various ion species and ion strengths in the solution to be measured. On the other hand, a rapid response of less than 100 s, a long lifetime of more than 1000 s and no contamination of the solution are also required for biochips to measure low level signals from trace amounts of solutions such as blood. Up-to-date research shows that liquid junction types[14–17] and nonliquid-junction types[18–20] have both merits and demerits in terms of quick response and lifetime. In the case of the liquid-junction-type, the cross section of the liquid junction region is responsible for the lifetime and response time. This can be achieved by careful control of the cross section with microfabrication technology. The nonliquid-junction type was fabricated only by placing a gas-permeable membrane on the electrode. However, both membrane quality and thickness are important to provide a long lifetime and a quick response. In this work, we have studied the fabrication of the non liquid-junction type reference electrode with PVC (polyvinyl chloride) as the membrane for our ion sensor.

Figure 9, it shows the structure of the new prototype nonliquid-junction type reference electrode. In the fabrication process, $SiO_2$/Si is used as a substrate, an 800 nm Ag layer is introduced and sputter-deposited on adhesive 50 nm Cr layer and chlorinated with 0.5 M $FeCl_3$ to form a Ag/AgCl electrode, which suggests a high sensitivity in comparison with the mixture solution of $K_2Cr_2O_7$ and HCl. Figure 10 shows the time dependence of the output voltages of the micro-reference electrode in 0.1 M PBS

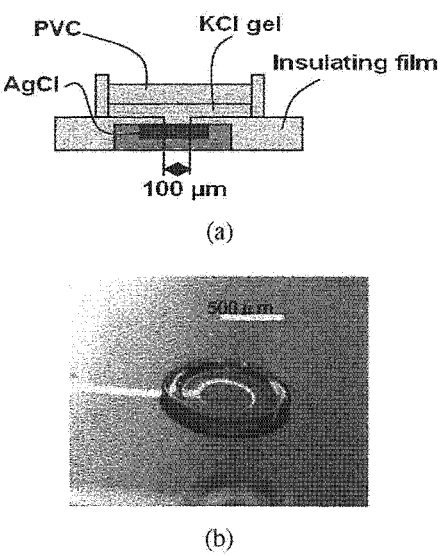


Fig. 9. Configuration of nonliquid-junction type reference electrode.

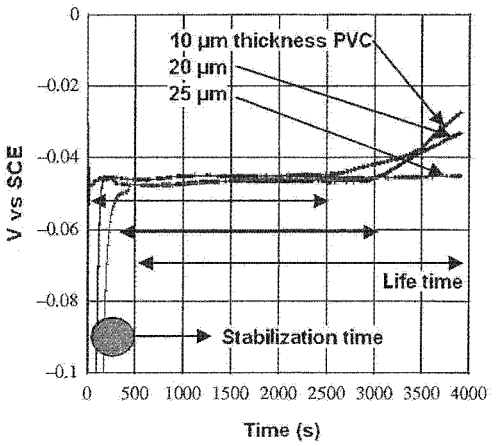


Fig. 10. Nonliquid-junction type reference electrode, showing results of quick stabilization time in the beginning with various PVC thicknesses in proportional to various lifetimes.

(phosphate buffer solution) for various PVC film thicknesses. The responses of all electrodes revealed the presence of the stabilization time until water arrived at the PVA+KCl layer and the saturated KCl layer was formed. During the measurement, the output voltage of −45 mV vs SCE (standard calomel electrode) in a saturated KCl layer was obtained. The stabilization time decrease with decreasing in the thickness as shown in Fig. 10. The interval during the output of −45 mV vs SCE shows the lifetime of the reference electrode. Over the interval, KCl diffuses gradually to the bulk solution through the film and the KCl concentration decreases, thereby increasing the potential. An adequate PVC membrane thickness has to be determined to obtain a membrane with longer lifetime for a shorter stabilization time; the thicker the membrane, the longer the lifetime. As a result thicknesses of 10 to 20 μm for the PVC film are adopted for our on-chip measurement.

## 4. Conclusions

In this study, health care chip BUN measurement based on detection ammonia ions using a TD19C6 ionophore PVC membrane has been achieved at a detection level as low as 1 mM in urea solution. Additionally, unlike conventional metal electrodes, the screen-printed Ag/AgCl electrodes have also been used throughout the experiments. From the results, it also suggests that screen-printed Ag/AgCl electrodes are suitable for potentiometic measurement. On the other hand, different from conventional liquid-based reference electrodes, key technologies to fabricate a nonliquid-junction type reference electrode have been demonstrated to achieve a rapid response of less than 100 s, a long lifetime of more than 1000 s and no contamination occurred in the measuring environment, which are required for biochips to measure low-level signals from trace amounts of solutions such as blood.

## Acknowledgements

This study was performed as a part of the Advanced Nano-Bio Device Project (P03011) supported by New Energy and Industrial Technology Development Organization (NEDO), Japan.

1) A. Manz, N. Graber and H. M. Widmer: Sens. Actuators B **1** (1999) 244.
2) D. R. Reyes, D. Lossifidis, P. Auroux and A. Manz: Anal. Chem. **74** (2002) 2623.
3) P. Auroux, D. Iossifidis, D. R. Reyes and A. Manz: Anal. Chem. **74** (2002) 2637.
4) Y. Horiike, S. Adachi, Y. Takamura, K. Kataoka, T. Ujiie and T. Ichiki: Int. Symp. Capillary Chromatogr., Gifu, Japan, 1999, OP409.
5) A. Oki, S. Adachi, Y. Takamura, K. Kataoka, T. Ichiki and Y. Horiike: Proc. μTAS 2000, Enschede, The Netherlands, 2000, p. 403.
6) A. Oki, S. Adachi, Y. Takamura, K. Ishihara, H. Ogawa, Y. Ito, T. Ichiki and Y. Horiike: Electrophoresis **22** (2001) 341.
7) A. Oki, M. Takai, H. Ogawa, Y. Takamura, T. Fukazawa, J. Kikuchi, Y. Ito, T. Ichiki and Y. Horiike: Jpn. J. Appl. Phys. **42** (2003) 3722.
8) A. Oki, H. Ogawa, M. Nagai, S. Shinbashi, M. Takai, A. Yokogawa and Y. Horiike: Mater. Sci. Eng. C **24** (2004) 837.
9) K. Suzuki, D. Siswanta, T. Otsuka, T. Amano, T. Ikeda, H. Hisamoto, R. Yashihara and S. Ohba: Anal. Chem. **72** (2000) 2200.
10) S. Sasaki, T. Amano, G. Monma, T. Otsuka, N. Iwasawa, D. Citterio, H. Hisamoto and K. Suzuki: Anal. Chem. **74** (2002) 4845.
11) J. Chin, C. Walsdorff, B. Stranix, J. Oh, H. J. Chung, S. M. Park and K. Kim: Angew. Chem., Int. Ed. Engl. **38** (1999) 2756.
12) T. Mock, D. Morrison and R. Yatscoff: Clin. Biochem. **28** (1995) 187.
13) M. Takai, S. Shinbashi, H. Ogawa, A. Oki, M. Nagai and Y. Horiike: Proc. Int. Symp. Fusion of Nano and Bio Technologies, 2003, Tsukuba, Japan.
14) H. Suzuki, T. Hirakawa, S. Sasaki and I. Karube: Sens. Actuators B **46** (1998) 146.
15) I. R. Lauks: Acc. Chem. Res. **31** (1998) 317.
16) H. Suzuki, H. Shiroishi, S. Sasaki and I. Karube: Anal. Chem. **71** (1999) 5069.
17) H. Suzuki, T. Hirakawa, S. Sasaki and I. Karube: Anal. Chim. Acta **387** (1999) 103.
18) D. Desmond, B. Lane, J. Alderman, J. D. Glennon, D. Diamond and D. W. M. Arrigan: Sens. Actuators B **44** (1997) 389.
19) H. J. Lee, U. S. Hong, D. K. Lee, J. H. Shin, H. Nam and G. S. Cha: Anal. Chem. **70** (1998) 3377.
20) T. Matsumoto, A. Ohashi and N. Ito: Anal. Chim. Acta **461** (2002) 253.

BOSTON
# μTAS 2005
MICRO TOTAL ANALYSIS SYSTEMS

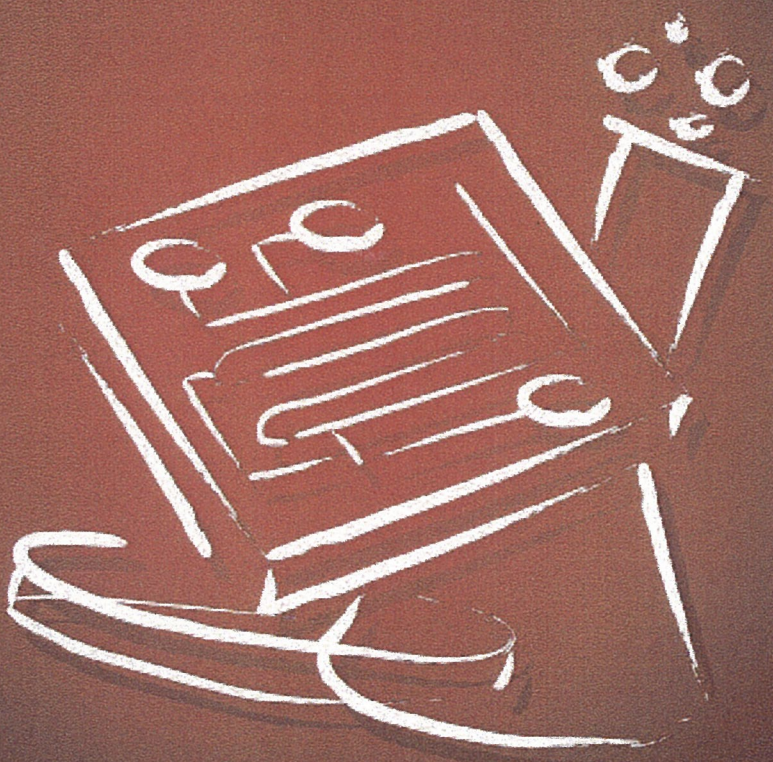

## Proceedings of μTAS 2005 Conference
## Volume 1

Ninth International Conference on Miniaturized Systems for Chemistry and Life Sciences
**October 9-13, 2005**
Boston, Massachusetts USA

Sponsored by

TRF
TRANSDUCER RESEARCH FOUNDATION

**Editors:** Klavs F. Jensen
Jongyoon Han
D. Jed Harrison
and Joel Voldman

**ISBN:** 0-9743611-1-9
**TRF CATALOG NUMBER:** 05TRF-0002

# SIMPLE AND QUICK DETECTION OF TARGET DNA BY HYBRIDIZATION IN NANO GAP CHANNEL ARRAY

**Shingi Hashioka, Ryo Ogawa, Akio Oki, Yuji Miyahara and Yasuhiro Horiike**
*National Institute for Materials Science, 1-1Namiki, Tsukuba, Ibaragi, 305-0044 JAPAN*

**Abstract**
The paper reports a simple and quick detection of target DNA by hybridization with a number of DNA trapped in nano gap channel array. A length of these T4 DNA fixed with stretching exceeds 20 μm in the channel. Subsequently, probe DNA was introduced into nano gap channel array to hybridize the trapped T4 DNA. When probe DNA is introduced after T4 DNA is trapped, intensive luminescence was observed in the channels. These results provide a simple and fast detection method of the target DNA originating from the infection disease.
**Keywords; DNA trap, hybridization, nano gap channel, probe DNA**

## 1. Introduction

We are studying a chip which enables us diagnose quickly the infection diseases by analysis of DNA obtained from lysis of cells. DNA extraction is one of the most important elements in this study. Especially, trapping technique of DNA with stretching in the micro channel is strongly required for the DNA detection. Washizu et al. succeeded in DNA stretching by using electroosmotic flow [1]. This paper reports a new DNA stretching method by using simple micro channel structure equipped with nano-gaps and then detection of target DNA by hybridization of probe DNA.

## 2. Experiments

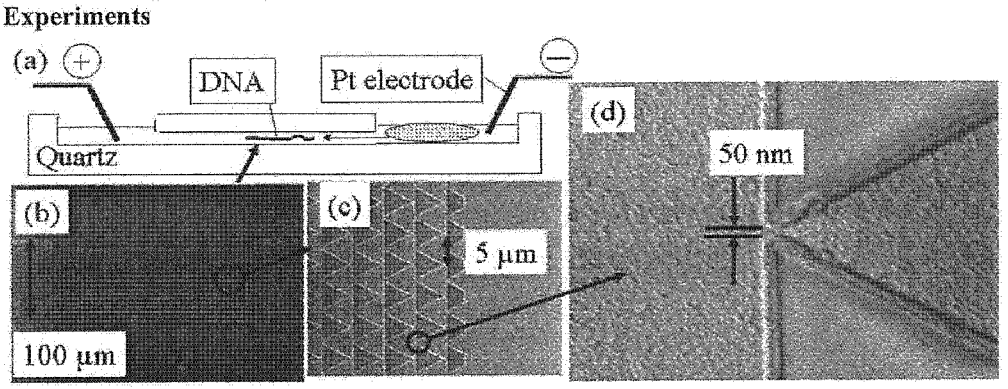


**Figure 1. (a) An illustration of the nano gap channel array. SEM images of (b) whole channel (c) array and (d) nano-gap.**

Figure 1 (a) shows an illustration of a DNA trapping chip, which is an analysis stage for our final goal. The 816 triangle shaped channels in an area of 85 x 240 $\mu m^2$, in which depth, maximum and minimum widths were 140 nm, 5μm and 50 nm, respectively, were fabricated on a quartz plate by an EB lithography and reactive ion etching processes. T4 DNA (166 kbps, length; about 50 μm) stained by YOYO-1, which was diluted by a TBE buffer solution, was introduced into the channel by electrophoresis using applied voltages of 50-100 V. All processes and measurements were carried out at a room temperature.


0-9743611-1-9/μTAS2005/$20©2005TRF

## 2. Results and discussions

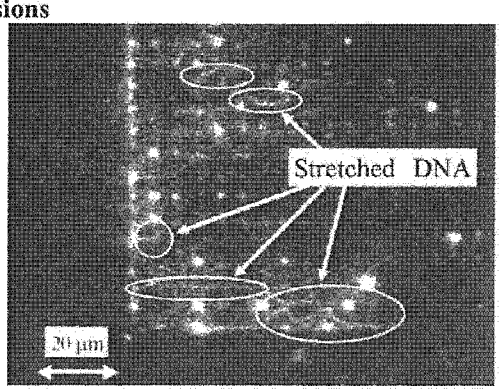


**Figure 2. Trapped DNA in the nano-gap channel array.**

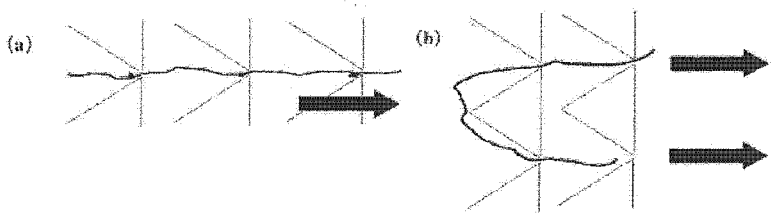


**Figure 3. Mechanisms of DNA trap (a) stretched straight (b) caught at two nano-gaps**

Figure 2 shows a fluorescence image of a number of DNA trapped at nano-gaps. When DNA rounded in a reservoir entered into the nano-gaps channel array, two type mechanisms were observed for the trappings. One was that DNA was stretched straight after caught at one nano-gap as shown in Fig. 3 (a). The other was that DNA strode over a triangle channel and then was stretched according to the manner in which both edges of DNA were caught at two nano-gaps as shown in Fig. 3 (b). A length of these DNA fixed with stretching exceeds 20 μm in the channel.

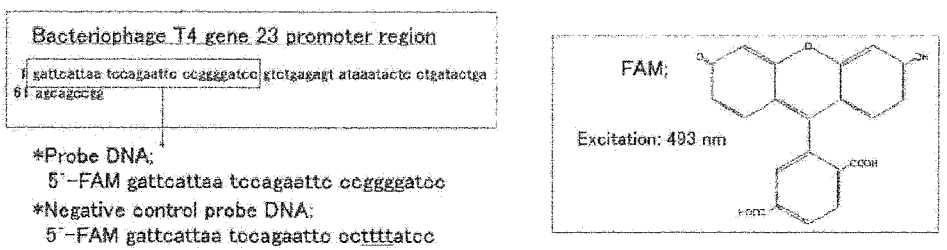


**Figure 4. Sequences of probe DNA and negative control probe DNA**

Subsequently, probe DNA was introduced from the reservoir into the nano-gaps channel array to hybridize the trapped DNA. The sequences of the probe DNA and the negative control DNA are shown in Table 1. A sequence of probe DNA is designed from parts of a sequence of Bacteriophage T4 gene. Negative control probe DNA is designed by the partially changed sequence to demonstrate an evidence of the hybridization of probe DNA.

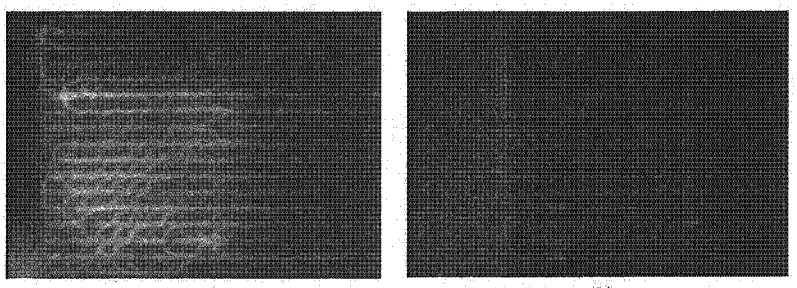


**Figure 5. (a) Introduction of probe DNA, (b) Introduction of negative control DNA**

Figure 5 (a) shows a fluorescent image, when probe DNA is introduced after trapping of T4 DNA. Intensive luminescence was seen in the channels. When negative control probe DNA was introduced, the luminescence was not observed as shown in Fig. 5 (b). These results provide a simple and quick detection method of the target DNA originating from the infection disease.

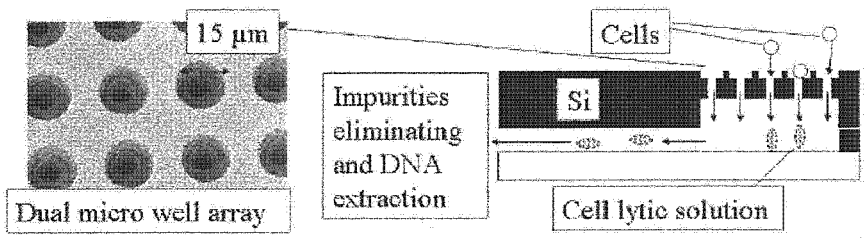


**Figure 6. Schematic view of the dual micro-well array.**

In order to achieve a diagnosis from cells, a dual micro-well array was developed for the cell lyses. The large wells with15 μm in diameter and 12 μm in depth were fabricated to trap cells such as lymphocytes. A cell lytic solution flows through the small well with 6 μm in diameter and 140 μm in depth. A filter to eliminate impurities before introduction of the solution into the nano-gaps channel array is now being developed. After that process, DNA is detected as mentioned above.

## 3. Conclusions

Simple and quick detection of target DNA by hybridization in nano gap channel array was demonstrated. It was observed that DNA trapped with stretching in nano gap channel array was hybridized with probe DNA. Additionally, dual micro-well array structure to trap cells and make lysis from them in the wells was fabricated. The chip system will allow us to analyze DNA from the cells lysis quickly, easily and safety in the near future.

## Acknowledgements

This study was performed as a part of the Advanced Nano-Bio Device Project (P03011) supported by NEDO (New Energy and Industrial Technology Development Organization). The authors would like to appreciate technical supports of Mr. Nao Nakagawa in University of Tsukuba to fabricate chips.

## References

[1] M. Washizu, Y. Nikaido, O. Kurosawa and H. Kabata, "Stretching yeast chromosomes using electroosmotic flow", Journal of Electrostatics, **57**, 395-405 (2003).

# WATER VISCOSITY AND HYDRODYNAMIC FLOW IN NANOPILLAR CHIPS

**N. Kaji[1], A. Oki[2], R. Ogawa[2], Y. Horiike[2] and Y. Baba[1, 3]**

*[1]Department of Applied Chemistry, Graduate School of Engineering, Nagoya University, [2]Biomaterials Center, National Institute for Materials Science, [3]Health Technology Research Center, National Institute of Advanced Industrial Science and Technology, JAPAN*

## ABSTRACT

Here we report an anomalous behavior of water, especially viscosity and hydrodynamic flow, in nanopillar chips. These physicochemical properties of water were investigated by single-particle tracking (SPT) technique. The results of diffusion constants of nanospheres indicated that a higher viscosity and a less hydrodynamic flow in nanopillar chips compared with a bulk solution.

**Keywords: Nanopillar, Single-Particle Tracking, Water Viscosity, Hydrodynamic Flow**

## 1. INTRODUCTION

We have demonstrated that nanopillar structures fabricated inside microchannels can work as a novel DNA sieving matrix [1]. In the process of developing DNA separation method using nanopillar chips, we found that several investigations for physicochemical properties in nanospace are necessary towards higher resolution and throughput. Since the surface areas of nanopillar chips are larger than simple channel structures, it is readily understood that such large charged surface areas raise complex electroosmotic flow and adsorption probability, and may affect the analysis [2]. Moreover, a water viscosity and a hydrodynamic flow in nanopillar chips might be potential factors affecting the performance. To develop these nanopillar chips as a novel nano-biodevice, it is indispensable to understand these fundamental phenomena in nanospace.

## 2. THEORY

Considering our experimental setup, Brownian motions of nanospheres were regard as quasi-two dimensional motion. Square displacements and mean square displacements should be calculated as a function of time:

$$[\quad _i(\ )]^2 = [\Delta\ _i(\ )]^2 \quad [\Delta x_i(t)]^2 \tag{1}$$

$$\left\langle R^2 \right\rangle \quad \frac{1}{N}\sum_{i=1}^{N}[\Delta =_i(t)]^2 \tag{2}$$

where $N$ is the total number of frames that have been traced. When the nanospheres undergo normal diffusion, the slope in $\left\langle\ ^2\right\rangle$ $\Delta R$ plot is linear and $\left\langle R^2\right\rangle$ can be expressed as following equation:

$$\left\langle\ ^2\right\rangle \qquad _x t D R\ D_x t = 4 \Box t \tag{3}$$

where $D$ is the two-dimensional diffusion coefficient. While the diffusion coefficient could be obtained experimentally, the Stokes-Einstein equation also provides the diffusion coefficient based on the thermodynamic and hydrodynamic views on diffusion by the following equation.

$$D = \frac{k_B T}{6\pi\eta r} \tag{4}$$



0-9743611-1-9/μTAS2005/$20©2005TRF